Model Predictive Control for isolated DC/DC converters with fast dynamic stabilization in DC microgrids

Linglin Chen
Department of Electrical and Electonics Engineering
University of Nottingham
Nottingham. United Kindom.
timzjuuon@gmail.com

Luca Tarisciotti
Facultad de Ciencias Fisicas y Matematicas,
Universidad de Chile
Santiago. Chile.
luca.tarisciotti@gmail.com

Alessandro Costabebber
Department of Electrical and Electonics Engineering
University of Nottingham
Nottingham. United Kindom.
ezzac1@exmail.nottingham.ac.uk

Pericle Zanchetta
Department of Electrical and Electonics Engineering
University of Nottingham
Nottingham. United Kindom.
eezpz@exmail.nottingham.ac.uk

Patrick Wheeler
Department of Electrical and Electonics Engineering
University of Nottingham
Nottingham. United Kindom.
eezpww@gmail.com

Tomislav Dragičević
Department of Energy Technology
Aalborg University
Aalborg. Denamrk.
tdr@et.aau.dk

***Abstract*— The proposed control for DC/DC converters with high frequency isolation, on one hand, provides fast stabilization to the DC microgrids without introducing additional passive components. On the other hand, it can improve load transition performance. Additionally a fixed switching frequency is maintained enabling easier passive components design. Moreover a minimal prediction horizon is utilized reducing the requirement on digital computational power. Simulations on a 270V/28V 100kHz 10kW Active-Bridge-Active-Clamp converter are carried out to verify the theoretical claims.**

Keywords*— *Model Predictive Control, Active-Bridge-Active-Clamp, system stabilization.

I. INTRODUCTION

Recently, there has been a great research interest in More Electric Aircraft (MEA). The research on active rectification technology in MEA has been taken place for years [1]–[3]. However, there are still aerial applications where line-commuted rectification is preferred due to reliability purposes [4], [5]. Therefore, stability issue when loaded with constant power load may occur [6].

T. Dragicevic [7] provided a comprehensive review on system damping methods, and proposed an active damping term based on Finite Control Set Model Predictive Control (FCS-MPC) to stabilize DC microgrids. However, this method is not applicable to isolated DC/DC power converters with high frequency transformers.

The applications of Model Predictive Control (MPC) in DC/DC converters are reported in [8]–[11]; *P. Karamanakos et al.* [8] proposed the implementation of FCS-MPC in a boost converter with the receding horizon. However this approach results in a larger current ripple than a PI-PWM based approach with the same sampling rate. *F. M. Oettmeier et al.* [9] have compared a Continuous Control Set MPC (CCS-MPC) with a hysteresis control in a boost converter. Although the dynamics performances are similar in the two control approaches, the voltage overshoot is completely avoided by using CCS-MPC control. *K. Z. Liu et al.* [10] implemented a single step prediction CCS-MPC with an outer PI loop to regulate the output voltage of a buck converter. This approach showed better response performance than a PI-PWM based control. *O. Yade et al.* [11] included switching loss and transformer current Root-Mean-Square (RMS) value into the cost function, and evaluate among different modulations. This approach can achieve optimal efficiency throughout the operation range, but the dynamic performance remains dominated by the PI control. Yet, none of the above mentioned literatures have applied MPC in a higher order and more complicated converter with high frequency transformer.

A number of different voltage standards co-exist for the DC electrical system on large civilian aircraft [12]. For example, 28VDC for powering avionics and other loads, 270VDC for power transmission. An isolated DC/DC power converter named Active-Bridge-Active-Clamp (ABAC) has been proposed for buffering between 270VDC and 28VDC [13].

In this paper, a Discretized Moving Control Set Model Predictive Control is proposed for the ABAC converter with the aim of controlling the LV side current, featuring fast system stabilization. It has the merits listed as follows:

1. Easy implementation on commercial control platforms;
2. Switching frequency is maintained fixed;
3. Fast system stabilization and load transition dynamics.

This paper is organized as follows: in Section II, the MEA application background is firstly introduced, and operation for the ABAC is explained. System stabilization with linear PI controllers is also introduced. After this, stability criteria is emphasized. In Section III, a discretized model for the ABAC converter is provided. The conceptual process of MDCS-MPC is introduced in development of the proposed cost function. In Section IV, Validations are presented for a 10 kW 100kHz 270V/28V ABAC converter.

II. BASIC OPERATION OF DAB

A. MEA background

A diagram of the power generation and distribution in MEA is shown in Fig. 1. Mechanical power is transformed into AC electric power through Permanent Magnet Synchronous Motors (PMSM). After that, three phase AC power is rectified by uncontrolled Diode Bridge into DC power and then fed onto the High Voltage (HV) DC voltage bus. A galvanically isolated DC/DC converter Active-Bridge-Active-Clamp (ABAC) is used to buffer between two DC terminals.

XXX-X-XXXX-XXXX-X/XX/$XX.00 ©20XX IEEE

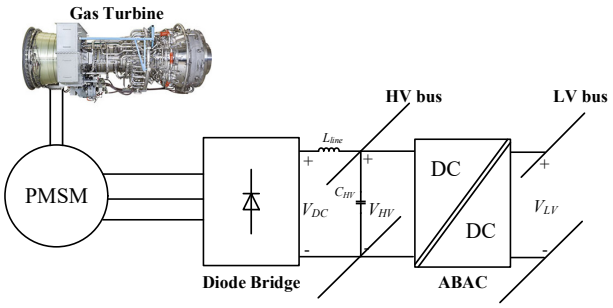

Fig. 1. A diagram of the DC power generation and distribution in MEA.

B. Conventional operation of the ABAC

The schematic of an ABAC converter is depicted in Fig. 2. The rectification stage is simplified by a DC source V_{DC} and its associated filters. Conceptual voltages and current waveforms on the high frequency transformer of the ABAC converter are illustrated in Fig. 3 [14]. The ABAC is operating under Single Phase Shift (SPS) [14], [15] where in one switching period T_s the duty cycles are fixed at 50%. The phase shift value $D_\varphi T_s$ is regarded as the only control variable.

The ABAC converter used in this application needs to have the ability to smoothly switch between the current mode and the voltage mode [16]. In the voltage mode, load voltage is regulated constant. In the current mode, load side current is controlled to reference. This paper uses current mode control only as an illustration of the proposed idea. Voltage mode control is rather similar, therefore, it has been omitted here.

In the illustration shown in Fig. 2, D_φ is composed of two parts: $D_{\varphi 1}$ and $D_{\varphi 2}$. The ABAC converter is controlled in the current mode where Low Voltage (LV) side current I_{LV} is regulated to a constant reference value I_{LVref}. Therefore, $D_{\varphi 1}$ is generated by the standard linear PI current control. $D_{\varphi 2}$ is the output of DC bus oscillation suppression loop [7] where high frequency oscillation on DC bus voltage is controlled zero. This control loop essentially changes the phase if the input impedance of the ABAC converter to improve the stability phase margin. This will be explained in the following subsection.

C. Stability criteria

Thevenin equivalent circuit of the DC distribution system is simplified as in Fig. 4. Z_{out} is the output impedance of a Diode Bridge, and Z_{in} is the input impedance of the ABAC converter. The DC bus voltage can then be expressed as:

$$V_{HV} = \frac{1}{1+\frac{Z_{out}}{Z_{in}}} V_{DC} \tag{1}$$

Therefore, the DC bus voltage is stable only if:

1) V_{DC} is stable, that is when unloaded, the Diode Bridge output voltage is stable.

2) The ratio Z_{out}/Z_{in} meets the Nyquist stability criteria [17].

The expression of Z_{out} can be easily derived based on the Thevenin equivalent approach as:

$$Z_{out} = \frac{L_l}{s^2 C_{HV} L_l + 1} \tag{2}$$

There are many ways to obtain the input impedance Z_{in} of the ABAC converter [17], [18]. However, the approach of the describing function is used in this paper [7]. The input impedance Z_{in} is largely dependent on the imposed control scheme. Using the linear PI control scheme shown in Fig. 2. The bode plots of Z_{in} and the Nyquist plots of the ratio Z_{out}/Z_{in} are presented in Fig. 5 and Fig. 6 using circuit parameters listed in Table I from Section IV.

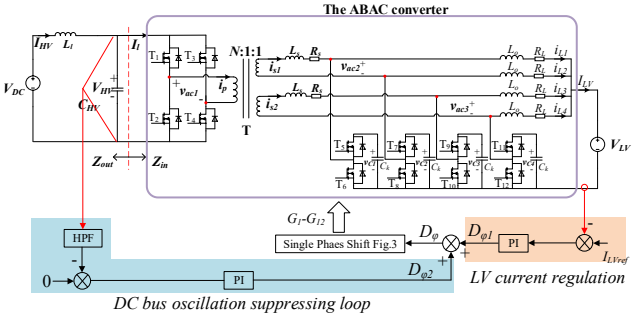

Fig. 2. The schematic of a current controlled ABAC converter with linear PI controllers.

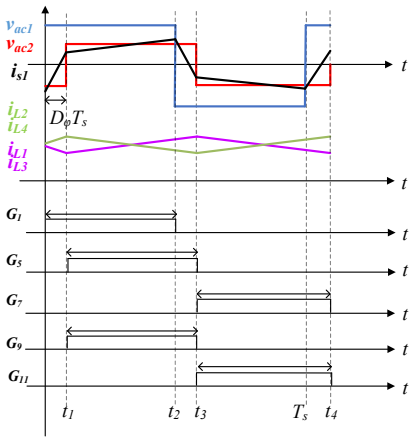

Fig. 3. Conceptual waveforms of the ABAC operating with SPS [14].

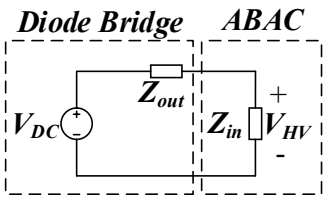

Fig. 4. Thevenin equivalent circuit of the DC distribution system in Fig. 2.

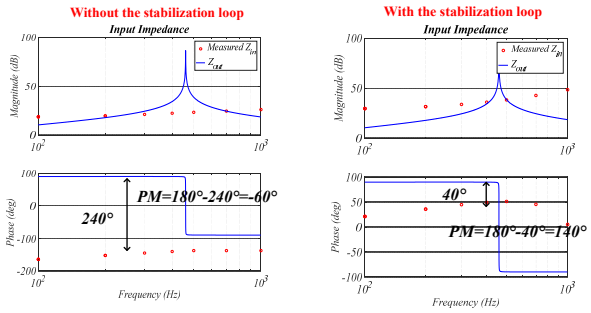

(a) (b)

Fig. 5. Bode plots of Z_{in} working under 5kW (a) without and (b) with the stabilization loop.

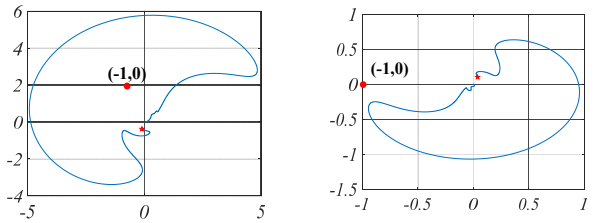

Fig. 6. Nyquist plots of the impedance ratio Z_{out}/Z_{in} working under 5kW (a) without and (b) with the stabilization loop.

It is clear from both the Nyquist plots and Bode plots that HV DC bus voltage can be stabilized with the linear controller. The phase margin is improved from unstable -70 degree to stable 150 degree. The above PI controlled ABAC is served as a comparison standard to the proposed controller.

III. The Proposed Model Predictive Control

The phase shift value between primary and secondary side voltages is divided into discretized values to fit the principle of FCS-MPC [19]. This method is novel however quite simple. Details will be given in the following subsections.

A. Modeling of the ABAC converter

In order to develop a switching average model, dynamics on the high frequency transformer and power transferring inductors (L_s) are neglected. A general switching average model can be derived as shown in Fig. 7 [20]. The aim of the designed controller is to regulate the output current I_{LV} to the desired reference value I_{LVref}.

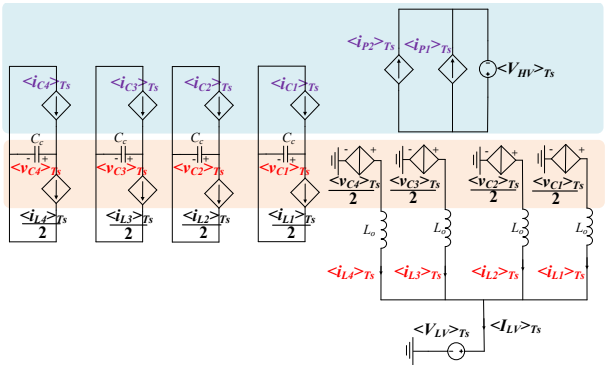

Fig. 7. The averaged model of the ABAC converter.

The discretised model of the ABAC is derived in [21]. Results are listed in (3) and (5).

$$I_{LV}[k+1] = \lambda_1 I_{LV}[k] + \lambda_2 I_{LV}[k-1] + \lambda_3 V_{HV}(1-D_\varphi)D_\varphi \tag{3}$$

$$\begin{aligned} V_{HV}[k+1] = {} & \beta_1 I_{HV}[k] + \beta_2 V_{HV}[k] \\ & + \beta_3 (I_{LV}[k] - I_{LV}[k-1])(1-D_\varphi[k])D_\varphi[k] \\ & + \beta_4 (1-D_\varphi[k])D_\varphi[k]V_{LV}[k] \end{aligned} \tag{4}$$

where,

$$\lambda_1 = 2 - \frac{T_s^2}{4C_c L_o} \quad \lambda_2 = -1 \quad \lambda_3 = \frac{T_s^3}{2NC_c L_o L_s} \tag{5}$$

$$\begin{cases} \beta_1 = \dfrac{T_s}{C_{HV}} \\ \beta_2 = 1 \end{cases} \qquad \begin{cases} \beta_3 = -\dfrac{L_o T_s}{2NC_{HV} L_s} \\ \beta_4 = -\dfrac{2T_s^2}{NC_{HV} L_s} \end{cases} \tag{6}$$

B. Operating principle of MDCS-MPC

The proposed Moving Discretised Control Set-Model Prediction Control (MDCS-MPC) regulates the converter current I_{LV} based on the discretized average model of the ABAC converter in (3). A preliminary cost function is proposed as in (7) with the only purpose of regulating current I_{LV} to the reference I_{LVref}. It is worth mentioning that (7) is not the ultimate cost function, but a simple one meant to help illustrate the operating principle of the proposed MDCS-MPC.

$$ct = (I_{LV\,ref} - I_{LV})^2 \tag{7}$$

It should be noted that the variable D_φ is continuous in nature. However, in digital control, D_φ needs to be discretized. The discretization precision is subjected to the control platform applied. Δ_f is defined as the finest phase shift value that can be achieved in a digital control platform. For bidirectional power flow, the ABAC works predominately in the range:

$$D_\varphi \in [-0.5, 0.5] \tag{8}$$

(8) is further discretized into μ_m (=$1/\Delta_f$+1) parts as described in (9).

$$D_\varphi \in \{-0.5, \cdots, 2\Delta_f, \Delta_f 0, \Delta_f, 2\Delta_f, \cdots, 0.5\} \tag{9}$$

In order to realize a control algorithm that is feasible on standard commercial microcontrollers, the proposed MDCS-MPC evaluates a reduced number of values in each sampling period. In one sampling period, μ ($\mu \le \mu_m$) number of points are assessed. They are centred at the previous working point.

An intuitive mechanism illustration of the proposed MDCS-MPC is depicted in Fig. 8. In the control interval k to k+1, μ=3 points are evaluated centred at the previous working point a. The current Discretized-Control-Set (DCS) is {a-Δ_f, a, a+Δ_f}. Value a+Δ_f results in the smallest cost function (ct), therefore, apply this value at time instance k+1. In the next control interval k+1 to k+2, the same process is repeated. However, the DCS has moved, and it now becomes {a, a+Δ_f, a+2Δ_f}. The DCS is moving with the working point within the domain of (9). In this control interval, value a+2Δ_f results in the smallest cost function (ct), therefore, this value is applied at the time instance k+2. This process goes on.

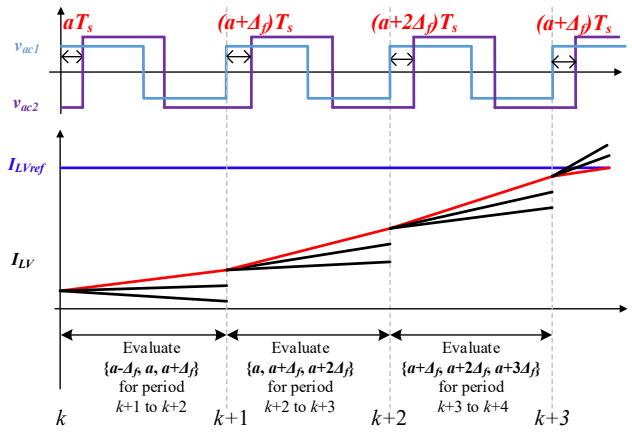

Fig. 8. The illustrative process of the proposed MDCS-MPC.

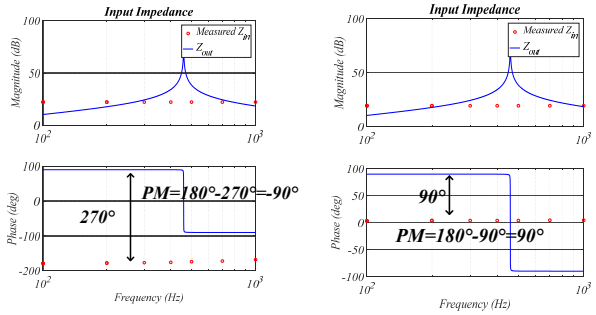

(a) (b)

Fig. 9. Bode plots of Z_{in} working under 5kW (a) without α_3=0 and (b) with α_3=50 the stabilization term.

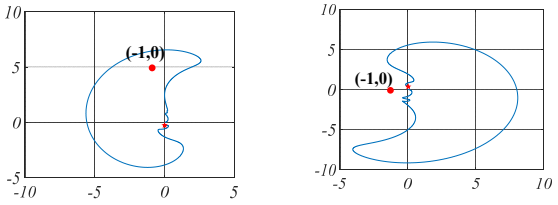

(a) (b)

Fig. 10. Nyquist plots of the impedance ratio Z_{out}/Z_{in} working under 5kW (a) without α_3=0 and (b) with α_3=50 the stabilization term.

C. Proposed cost function

Taking into account the computational delay, MDCS-MPC has a prediction horizon of two sampling periods. Therefore, the cost function is proposed as follows:

$$ct = \alpha_1 G_1 + \alpha_2 G_2 + \alpha_3 G_3 \tag{10}$$

where,

$$\begin{cases} G_1 = (I_{LV\,ref} - I_{LV}[k+2])^2 \\ G_2 = (I_{LV}[k+2] - I_{LV}[k])^2 \\ G_3 = (V_{HV}[k+2] - V_{HV}^{DC}[k+2])^2 \end{cases} \tag{11}$$

The first term is responsible for the regulation of LV current. The second term reduces the dithering phenomenon due to sampling noise. The third term takes charge in DC oscillation suppressing. The third term potentially alters the input impedance of the ABAC converter. The stability analysis is provided in the following subsection.

D. Impedance & stability

The impedance of the ABAC controlled by PI controllers can be derived from small signal modelling [18], however, when non-linear controller is used, the conventional modelling approach is not applicable. *T. Dragicevic* [19] proposed a describing function approach to evaluate the impedance of the converter controlled by MPC. This approach is also adopted in this paper. The Bode plots of Z_{in} and the Nyquist plots of the ratio Z_{out}/Z_{in} are presented in Fig. 9 and Fig. 10 using circuit parameters listed in Table I from Section IV. Fig. 9 (a) shows that when ABAC is regulated by the proposed MDCS-MPC, the converter shows the behaviour of constant power load where the phase of Z_{in} keeps -270 degree at the low frequency range. It is noted that when the damping term is enabled as shown in Fig. 9 (b) the phase margin is improved from -90 to 90. The Nyquist plots in Fig. 10 describes the fact that the point (-1,0) is not encircled anymore when the damping term is enabled, which means the system is stable after the damping function is inserted.

IV. Validation Results

The circuit of the ABAC is designed and implemented in software PLECS embedded in Simulink MATLAB. The MDCS-MPC is implemented as shown in flow chart Fig. 11. Note that μ can be set greater than 3 for faster dynamic if enough computation power is provided. However, in our case, the sampling/switching frequency 100kHz is already high enough to ensure a high bandwidth. Therefore, a minimal DCS is used where μ equals to 3. HV voltage V_{HV}, LV voltage V_{LV} and current I_{LV} are measured. LV current I_{LV} is regulated to I_{LVref}. Outputs of both PI and MDCS-MPC controllers are considered to be the phase shift D_φ in Fig. 3. Weighting factors are set as α_1=1, α_2=2, α_3=50 in all simulations for MDCS-MPC.

A. Load transition

The load transitions are shown in Fig. 12 (a)-(c). The PI controllers are designed and tuned using approaches described in [22]. Notably the switching harmonics are cancelled in I_{LV} as shown in Fig. 12 (a). The transition time for load step up Fig. 12 (b) and down Fig. 12 (c) are 4.5ms and 4ms respectively.

TABLE I
ABAC CONVERTER PARAMETERS

Symbol	Description	Value
V^*_{HV}	Nominal HV voltage	270V
V^*_{LV}	Nominal LV voltage	28V
P^*	Rated power	10 kW
f_s	Switching frequency	100 kHz
N	Transformer turn ratio	5
C_{HV}	Input capacitance	24 uF
C_c	Clamp capacitance	150 uF
L_s	Power transfer inductance	500 nH
L_l	Filter inductance	5 mH
L_o	Output inductance	1.65 uH

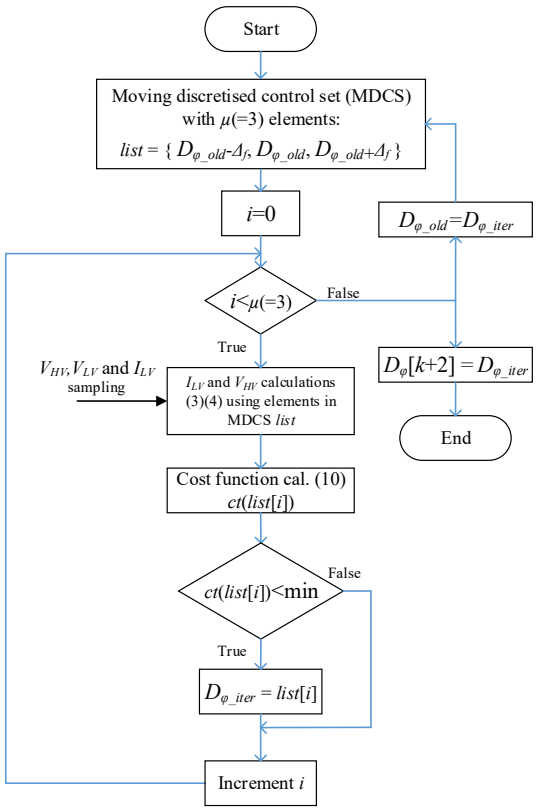

Fig. 11. The flow chat of the proposed MDCS-MPC.

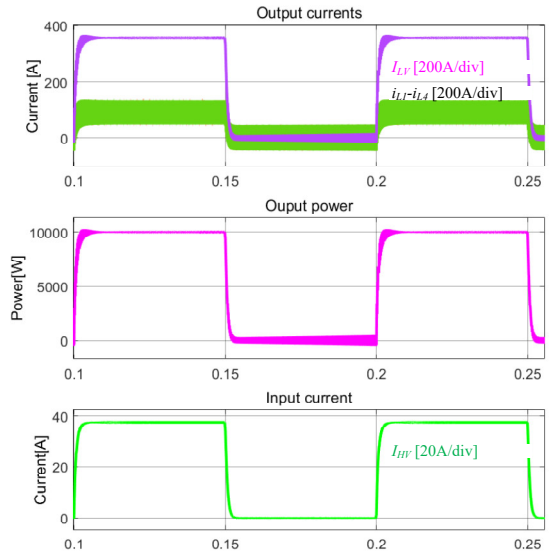

(a)

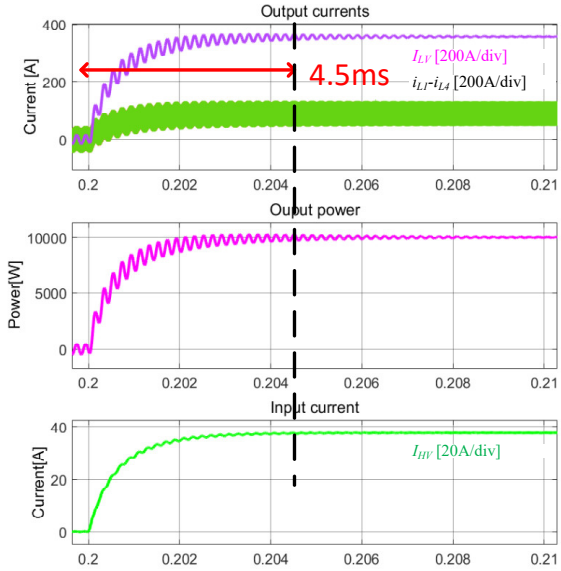

(b)

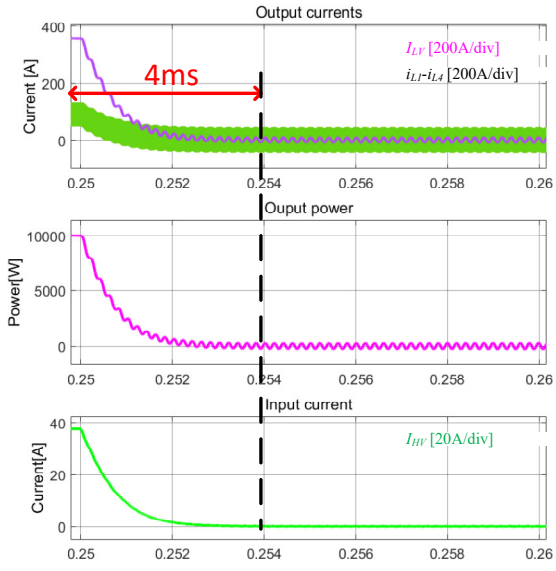

(c)

Fig. 12. Load transition with PI controllers.

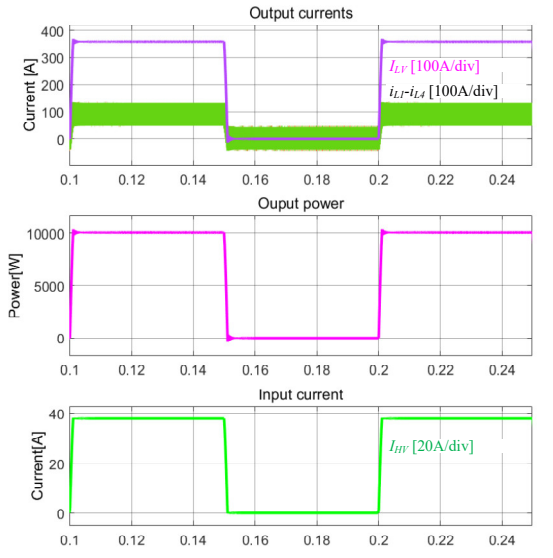

(a)

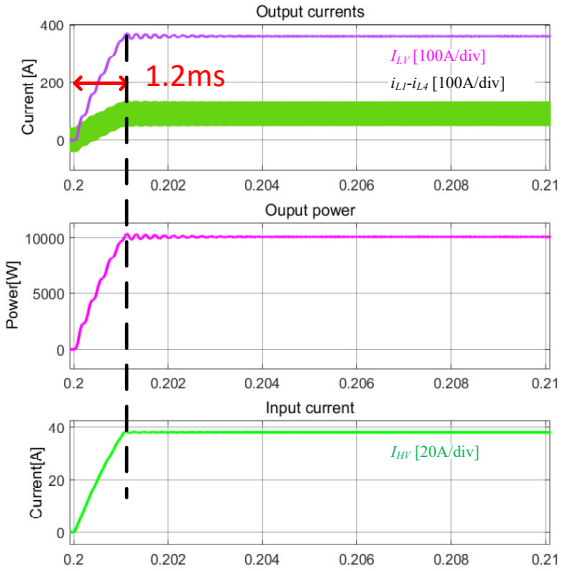

(b)

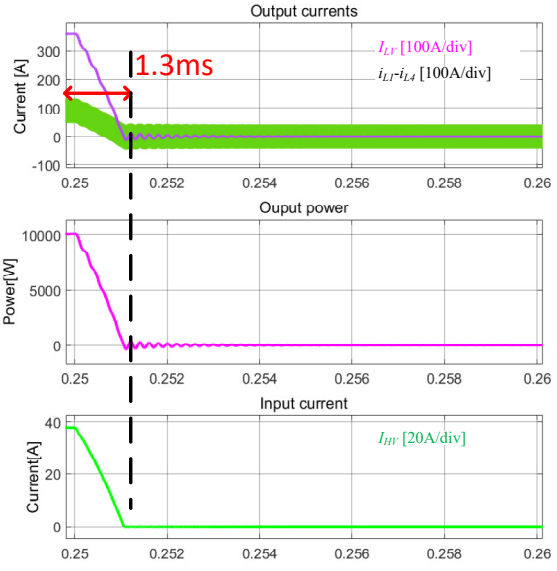

(c)

Fig. 13. Load transition with the MDCS-MPC controller.

The load transitions are shown in Fig. 13 (a)-(c) with the control of MDCS-MPC. The transition time for load step up Fig. 13 (b) and down Fig. 13 (c) are 1.2ms and 1.3ms respectively. It is clear that with the proposed control approach, the load transition is improved by at least 67.5%. It is worth mentioning that the ability of MDCS-MPC can still be pushed further if μ can be increased providing enough computational power is given.

B. *Stabilization of the DC bus voltage*

Comparison for DC stabilization is shown in Fig. 14. Fig. 14 (a) shows the effectiveness of the damping control loop using PI controllers as mentioned in Fig. 2. The HV DC voltage bus is stabilized after the damping loop is enabled as confirmed also in the Nyquist plot Fig. 6. It takes 30ms to stabilize the V_{HV}. However, when MDCS-MPC is used, after the damping term is enabled, the oscillation in V_{HV} is suppressed effectively. Moreover, MDCS-MPC achieves much faster stabilization process than PI controllers as validated in Fig. 14 (b).

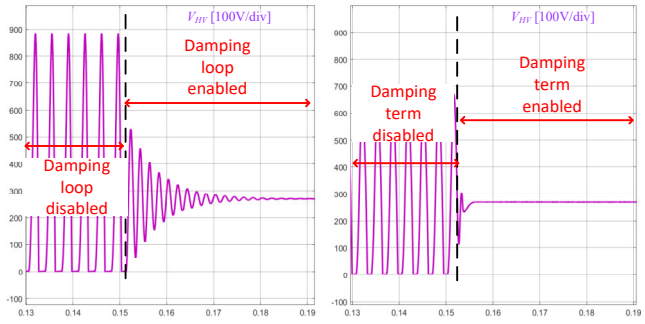

(a) (b)

Fig. 14. Comparison between stabilization dynamics between (a) PI controllers and the (b) MDCS-MPC controller.

V. Conclusion

The MDCS-MPC is proposed in this paper. On one hand, it provides fast load transition; On the other hand, it can achieve fast system stabilization. Moreover, Implementation of this controller is fairly simple. The calculation burden is much reduced compared to a long prediction horizon approach [23]. The proposed control features fixed switching frequency which eases the passive components design.

References

[1] C. Li *et al.*, "A Modified Neutral-Point Balancing Space Vector Modulation Technique for Three-Level Neutral Point Clamped Converters in High Speed Drives," *IEEE Trans. Ind. Electron.*, pp. 1–1, 2018.

[2] S. Bozhko *et al.*, "Development of Aircraft Electric Starter–Generator System Based on Active Rectification Technology," *IEEE Trans. Transp. Electrif.*, vol. 4, no. 4, pp. 985–996, Dec. 2018.

[3] Z. Huang, T. Yang, P. Wheeler, M. Galea, P. Giangrande, and S. Chowdhury, "An Active Modulation Scheme to Boost Voltage Utilisation of the Dual Converter with a Floating Bridge," *IEEE Trans. Ind. Electron.*, pp. 1–1, 2018.

[4] A. Nasr, S. Hlioui, M. Gabsi, M. Mairie, and D. Lalevee, "Design Optimization of a Hybrid-Excited Flux-Switching Machine for Aircraft-Safe DC Power Generation Using a Diode Bridge Rectifier," *IEEE Trans. Ind. Electron.*, vol. 64, no. 12, pp. 9896–9904, Dec. 2017.

[5] S. Jordan and J. Apsley, "Open-circuit fault analysis of diode rectified multiphase synchronous generators for DC aircraft power systems," in *2013 International Electric Machines & Drives Conference*, 2013, pp. 926–932.

[6] A. Emadi, A. Khaligh, C. H. Rivetta, and G. A. Williamson, "Constant Power Loads and Negative Impedance Instability in Automotive Systems: Definition, Modeling, Stability, and Control of Power Electronic Converters and Motor Drives," *IEEE Trans. Veh. Technol.*, vol. 55, no. 4, pp. 1112–1125, Jul. 2006.

[7] T. Dragicevic, "Dynamic Stabilization of DC Microgrids with Predictive Control of Point of Load Converters," *IEEE Trans. Power Electron.*, pp. 1–1, 2018.

[8] P. Karamanakos, T. Geyer, and S. Manias, "Direct model predictive current control of DC-DC boost converters," in *2012 15th International Power Electronics and Motion Control Conference (EPE/PEMC)*, 2012, p. DS2c.11-1-DS2c.11-8.

[9] F. M. Oettmeier, J. Neely, S. Pekarek, R. DeCarlo, and K. Uthaichana, "MPC of Switching in a Boost Converter Using a Hybrid State Model With a Sliding Mode Observer," *IEEE Trans. Ind. Electron.*, vol. 56, no. 9, pp. 3453–3466, Sep. 2009.

[10] K. Z. Liu and Y. Yokozawa, "An MPC-PI approach for buck DC-DC converters and its implementation," in *2012 IEEE International Symposium on Industrial Electronics*, 2012, pp. 171–176.

[11] O. Yade, J.-Y. Gauthier, X. Lin-Shi, M. Gendrin, and A. Zaoui, "Modulation strategy for a Dual Active Bridge converter using Model Predictive Control," in *2015 IEEE International Symposium on Predictive Control of Electrical Drives and Power Electronics (PRECEDE)*, 2015, pp. 15–20.

[12] M. Tariq, A. I. Maswood, C. J. Gajanayake, and A. K. Gupta, "Aircraft batteries : current trend towards more electric aircraft," *IET Electr. Syst. Transp.*, vol. 7, no. 2, pp. 93–103, 2017.

[13] L. Chen, L. Tarisciotti, A. Costabeber, Q. Guan, P. Wheeler, and P. Zanchetta, "Phase-Shift-Modulation for a current-fed isolated DC-DC converter in More Electric Aircraft," *IEEE Trans. Power Electron.*, pp. 1–1, 2018.

[14] L. Chen, L. Tarisciotti, A. Costabeber, F. Gao, P. Wheeler, and P. Zanchetta, "Advanced modulations for a current-fed isolated DC-DC converter with wide voltage operating ranges," *IEEE J. Emerg. Sel. Top. Power Electron.*, pp. 1–1, 2018.

[15] L. Tarisciotti, A. Costabeber, L. Chen, A. Walker, and M. Galea, "Current fed isolated DC/DC converter for future aerospace microgrids," *IEEE Trans. Ind. Appl.*, pp. 1–1, 2018.

[16] Y. Zhu, B. Xu, L. Chen, D. Dong, P. Lin, and D. Xu, "Multi-Functional Bidirectional AC/DC T-type 3-Level Converter for Super UPS," in *2014 International Power Electronics and Application Conference and Exposition*, 2014, pp. 390–395.

[17] J. Sun, "Impedance-Based Stability Criterion for Grid-Connected Inverters," *IEEE Trans. Power Electron.*, vol. 26, no. 11, pp. 3075–3078, Nov. 2011.

[18] R. Ahmadi, D. Paschedag, and M. Ferdowsi, "Closed-loop input and output impedances of DC-DC switching converters operating in voltage and current mode control," in *IECON 2010 - 36th Annual Conference on IEEE Industrial Electronics Society*, 2010, pp. 2311–2316.

[19] T. Dragicevic, "Model Predictive Control of Power Converters for Robust and Fast Operation of AC Microgrids," *IEEE Trans. Power Electron.*, vol. 33, no. 7, pp. 6304–6317, Jul. 2018.

[20] L. Chen, L. Tarisciotti, A. Costabeber, P. Zanchetta, and P. Wheeler, *Parameters mismatch analysis for the Active-Bridge-Active-Clamp (ABAC) converter*. IEEE, 2017, pp. 1–6.

[21] L. Chen, L. Tarisciotti, A. Costabeber, P. Wheeler, and P. Zanchetta, "Model Predictive Control for Isolated DC/DC Power Converters with Transformer Peak Current Shaving," in *2018 IEEE Energy Conversion Congress and Exposition (ECCE)*, 2018, pp. 5954–5960.

[22] Karl J. Åström and T. Hägglund, *Advanced PID control*. ISA-The Instrumentation, Systems, and Automation Society, 2006.

[23] P. Karamanakos, T. Geyer, and S. Manias, "Direct Voltage Control of DC–DC Boost Converters Using Enumeration-Based Model Predictive Control," *IEEE Trans. Power Electron.*, vol. 29, no. 2, pp. 968–978, Feb. 2014.